An Optoelectronics-Based Sensor for Measuring Multi-Axial Shear Stresses

Michael A. McGeehan, Salil S. Karipott, Michael E. Hahn, David C. Morgenroth, Keat G. Ong

***Abstract*—There is an increasing need for tactile shear sensors, particularly for medical applications such as orthopedic rehabilitation. Examples include measuring interfacial shear stresses between a residual limb and prosthesis to monitor socket fit and improve residual limb tissue health, and tracking shearing between a foot and shoe for assessing performance in athletes. However, there are considerable challenges in implementing shear force sensors for orthopedic applications due to the requirements for noninvasiveness, low mass, low power, and robustness against motion artifacts, normal force, and/or electromagnetic fields. To address these challenges, we designed, fabricated, and characterized a simple, low-cost, optoelectronic sensor that can measure multi-axial shear stresses. This novel sensor is based on a red, green, and blue (RGB) light-emitting diode (LED) projecting a cyclic illumination of RGB light onto a color pattern surface. As shear strain causes a displacement between the LED and the color pattern, the intensities of the reflected lights change due to the shift of the color pattern position. A photodiode captures the reflected light intensity at each color illumination, allowing the determination of the color pattern surface displacement and the shear along two axes. In this paper, we also report the efficacy of the sensor under benchtop testing conditions, confirming the potential of this technology for shear monitoring in orthopedic devices such as protheses or shoes. Future efforts will focus on miniaturization and packaging of the sensors, and characterizing their performance for the aforementioned medical applications.**

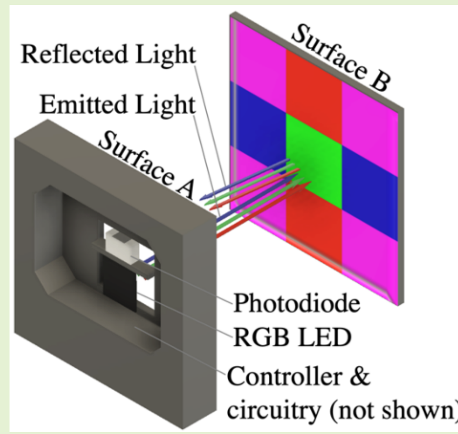

***Index Terms*—Shear force, strain, displacement, optical sensors, orthopedic rehabilitation, prosthesis.**

I. Introduction

The need for tactile shear sensors is rapidly increasing, particularly for robotics and medical applications [1,2]. Within the field of robotics, shear sensors are useful for detecting slippage in grasping devices or ground contact dynamics in walking devices [1]. Among the many medical areas, the use of these sensors in orthopedic rehabilitation, such as measuring interfacial shear stresses between a residual limb and prosthetic socket, have been found to be impactful for managing socket fit and residual limb tissue health [3–5]. Furthermore, measurement of shearing between the plantar surface of a foot and shoe could lead to new innovations for assessing performance in athletes or managing tissue ulceration among individuals with diabetic neuropathy and/or dysvascular conditions. However, there are considerable challenges in implementing shear force sensors for orthopedic applications due to the specific requirements and constraints; shear sensors designed for the aforementioned uses should be mechanically imperceptible to the user and therefore must be packaged in a flexible housing and/or adopt a small footprint. In addition, the sensor must have low mass, low power requirements, and be relatively unaffected by motion artifacts, normal force, and/or electromagnetic fields.

Many existing shear sensors are based on capacitive sensing principles [3–9], which often necessitate bulky packaging and are sensitive to electromagnetic interference from the environment, nearby mechatronic systems, or the human body. For example, Sanders and Daly [4] used metal-foil strain gauges embedded in the wall of a prosthetic socket to measure residual limb-prosthetic socket interfacial shear stresses. However, the bulk and mass of these sensors necessitated that holes be cut in the wall of socket, thus limiting their usefulness in clinical or daily use settings. Cheng et al. [6] developed a polymer-based capacitive sensing array for normal and shear force measurement in robotics and orthopedics. This design is more flexible but has a larger footprint than the metal-

This project is partially supported by the University of Oregon Venture Launch's Translation Research Grant and University of Oregon's Knight Campus Start Up fund.

M. A. McGeehan is with the Phil and Penny Knight Campus for Accelerating Scientific Impact, University of Oregon, OR 97403, USA (e-mail: mmcgeeha@uoregon.edu).

S. S. Karipott is with the Phil and Penny Knight Campus for Accelerating Scientific Impact, University of Oregon, OR 97403, USA (e-mail: karipott@uoregon.edu).

M E. Hahn is with the Department of Human Physiology, University of Oregon, OR 97403, USA (e-mail: mhahn@uoregon.edu).

D. C. Morgenroth is with the VA RR&D Center for Limb Loss and Mobility (CLiMB) and the Department of Rehabilitation Medicine, University of Washington, Seattle, WA 98108, USA (e-mail: dmorgen@uw.edu).

K. G. Ong is with the Phil and Penny Knight Campus for Accelerating Scientific Impact, University of Oregon, OR 97403, USA (e-mail: kgong@uoregon.edu).

foil strain gauges. It also offers a relatively limited shear sensing capacity (<1 N), making it impractical for many robotic and orthopedic applications. Laszczak et al. [3,5] developed a 3D-printed capacitive shear stress sensor. This sensor has a miniaturized design (20 mm × 20 mm × 4 mm), but is unable to differentiate between shear stresses along different axes.

In contrast to capacitive designs, optoelectronic sensors are advantageous for measuring shear stress because they are generally thinner and are relatively unaffected by magnitude of normal force [10]. Furthermore, devices based on optical sensing principles are unaffected by electromagnetic interference induced by the surroundings, the human body, or other devices interacting with the sensor. A thin optical tactile shear sensor was developed and validated in [10–13]. This device senses shear stress based on optical coupling between a Vertical-Cavity Surface-Emitting Laser (VCSEL) and a photodiode separated by a transparent elastomeric transducer layer. The sensor exhibited a repeatable sigmoidal relationship between photodiode current and shear stress for stresses up to 5 N. While these studies made important progress towards the use of optical-based sensing techniques for measuring shear stress, the limited range of shear sensing, high power required to drive the VCSEL, and inability to measure directionality of shear stresses limit its use for robotics and medical applications.

There remains a need for a miniaturized optical-based shear stress sensor with a scalable design that can be tuned to sense shearing of different magnitudes. The sensor should also be capable of differentiating directionality of the shear stresses and require low power. This paper describes the design, fabrication, and characterization of a simple, low-cost, optoelectronic sensor for measuring multi-axial shear stresses. We characterized the performance of this novel sensor under benchtop testing conditions; future efforts will focus on miniaturization and packaging of the sensors, and characterizing their performance for shear monitoring in orthopedic devices such as prostheses or shoes.

II. Methods

A. Operational Principle

The sensor measures multi-axial shear stresses based on optical coupling between a red, green, and blue (RGB) light-emitting diode (LED) and a photodiode. This is a contactless design, meaning that all electronics and wiring are confined to one side of the sensor. A schematic of the sensing principle is shown in Figure 1. The instrumented side of the sensor has a windowed pattern (Figure 1A, Surface A), whereas the opposite side of the sensor (Figure 1A, Surface B) displays a colored grid consisting of green, red, blue, and magenta (red + blue) panels. Red, green, blue, and magenta color panels were selected due to their ability to selectively absorb or reflect corresponding colors emitted from the LED. The contactless design offers versatility in how the sensor is implemented. For example, the pattern on Surface B could be printed on a second sensor component as in Figure 1, or on an adjacent stationary surface or existing device (e.g., a shearing body on a robot). Controlling electronics cycle the LED color while reflected light intensity is measured via resistance at the photodiode during red (R_r), green (R_g), and blue (R_b) light illumination. The photodiode acts as a variable resistor in response to light intensity and thus, variations in red, green, and blue light intensities are measured via voltage changes at the photodiode during red, green, or blue illumination.

When there is no shear force applied to the sensor, Surfaces A and B are perfectly aligned, and thus only green appears in the window on Surface A (Figure 1B, lower left). Under this condition, the photodiode only measures a resistance change when the LED is emitting green light, since there is no blue or red color surface to reflect the blue and red lights, respectively ($R_g > 0, R_r = R_b = 0$). A vertical shear force causes misalignment of Surfaces A and B, and the red squares on Surface B are exposed through the window of Surface A (Figure 1B, lower middle-left), leading to resistance changes in R_g and R_r. The values for R_g and R_r are inversely proportional and proportional to the magnitude of vertical shear force, respectively. Similarly, a horizontal shear force causes the blue on Surface B to be visible in the window on Surface A (Figure 1B, lower middle-right). When the sensor experiences both vertical and horizontal shear forces, the magenta surface appears through the opening of Surface A (Figure 1B, lower right), which reflects both blue and red lights. As a result, vertical shear force can be calculated as the ratio R_r / R_g, and horizontal shear force can be determined as R_b / R_g.

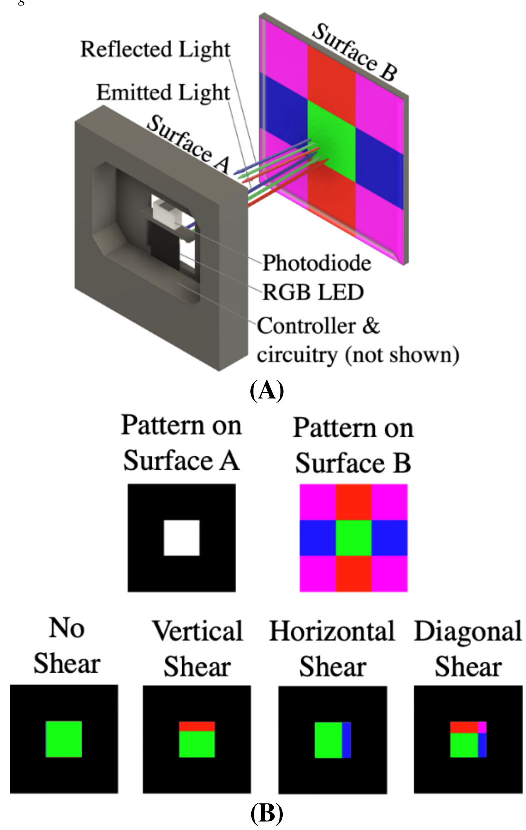

Figure 1. (A) Illustration of the operational principle of the contactless optoelectronic shear sensor. **(B)** Schematic diagram of shear sensing principle based on optical coupling between the RGB LED and photodiode.

B. Sensor Architecture and Fabrication

The sensor is comprised of three main components: an instrumented housing for the LED, photodiode, and circuitry; a color pattern (Surface B) and a black trim window (Surface A); and an intermediate optically clear deformable layer made of polydimethylsiloxane (PDMS) elastomer layer (Sylcap, MicroLubrol, Clifton, NJ) separating Surfaces A and B (Figure 2). The sensor packaging, including circuitry, is 15 mm × 15 mm × 5 mm (thickness). The thickness of the sensor is largely dependent upon the thickness of the deformable layer – the thicker the layer, the larger the sizes for Surfaces A and B. The maximum range and sensitivity towards shear stress can be tuned by changing the PDMS thickness and curing conditions, which affects the stress-strain property of the material [14].

The LED (DotStar APA102-2020, Shenzhen LED Color Opto Electronic Co., Shenzhen, China) is 2 mm × 2 mm × 0.9 mm and emits red, green, and blue lights at 620 nm, 520 nm, and 465 nm wavelengths, respectively. At 20 mA, the brightness for these colors is 300-330 mcd (millicandela), 420-460 mcd, and 160-180 mcd. The photodiode (Vishay Semiconductors, VEMD1060X01, Shelton, CT) is 1 mm × 2 mm × 0.9 mm with a 0.2 mm^2 active area. The photodiode is sensitive to wavelengths ranging from 350 nm to 1070 nm, which are inclusive of the red, green, and blue color spectra. The LED and photodiode are mounted to a printable circuit board (PCB) (OshPark, Lake Oswego, OR) which is housed in a 3D printed methylacrylate photopolymer resin (Figure 2). By employing rapid prototyping technology in the fabrication process, the sensor's cost-efficiency and versatility are improved. Within the housing, the LED and photodiode are isolated such that the photodiode is only exposed to light reflected from Surface B. Surface B consists of a 3D printed plate. The color pattern (Figure 1B) was printed on an adhesive-backed vinyl with a matte finish (JukeBox Prints Inc., Toronto, Canada). This finish has a 4-5 year durability rating and is resistant to oil and water penetration.

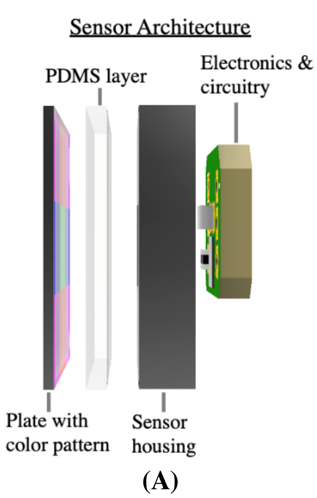

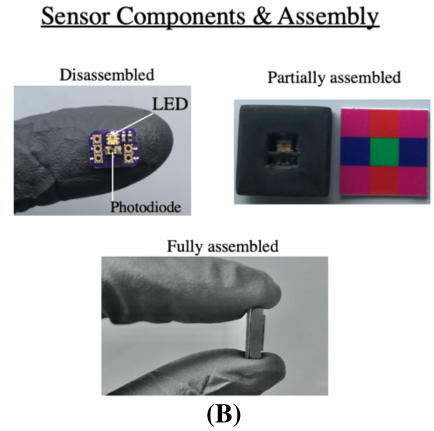

Figure 2. (A) 3D illustration of the sensor components. **(B)** Partially populated circuit board for the sensor featuring the LED and photodiode (left); partially assembled sensor without elastomer layer (right); and fully-assembled sensor and circuitry (bottom).

A resin mold for the PDMS elastomer layer (Sylcap, Microlubrol, Clifton, NJ) was 3D printed and adhered to a Teflon plate. The base agent and curing agent were poured into the mold and cured at room temperature for 24 hrs. After curing, the PDMS elastomer was removed from the mold, trimmed to the dimensions of the sensor housing, and adhered to Surfaces A and B of the sensor (Loctite 401, Düsseldorf, Germany). The mass of the as-fabricated sensor was 1.01 g. In previous material characterization studies, the shear modulus of PDMS at room temperature was found to be 250 – 450 kPa [10,15]. However, the material properties of PDMS are known to be tunable by adjusting the geometry and curing parameters of the elastomer [14]. A flow diagram of the sensor fabrication and validation processes are depicted in Figure 3.

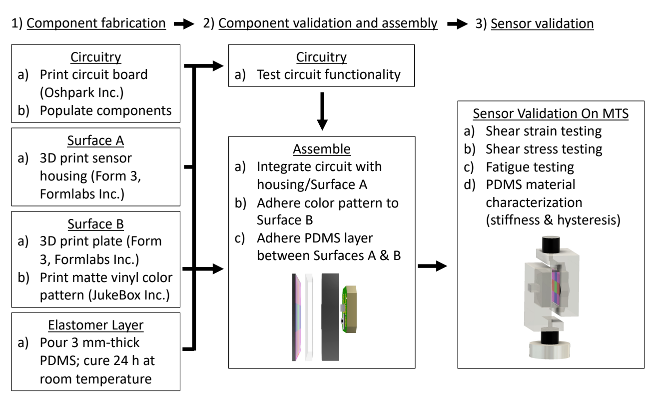

Figure 3. Flow diagram of sensor fabrication and validation processes.

C. Sensor characterization

The sensor's response to both displacement and applied shear force were measured. Measuring the response to displacement serves to establish the sensitivity of the sensor towards change in strain. Measuring the response to shear stress is useful to further characterize the sensor's performance under the ultimate use conditions.

To apply controlled displacements (i.e., shear strains), a 3D-printed housing was designed to secure the sensor components in a materials testing system (EnduraTEC ELF, TA Instruments, New Castle, DE) (Figure 3). A 3-mm thick spacer was placed between the two sides of sensor in place of the elastomer. Surface B was displaced with respect to the instrumented side of the sensor (Surface A) in 1 mm increments up to 10 mm. At each 1 mm position, a static measurement of RGB color intensity was recorded by cycling each LED color 10 times at 50 Hz and recording the average of the 10 measurements for each color. To measure the repeatability of the sensor, 5 trials were completed, and inter-trial variability was calculated. These measurements were then repeated in the horizontal direction. Sensor-derived measurements of displacement were then compared to measurements from the materials testing system's integrated High Accuracy Displacement Sensor (HADS) (EnduraTEC ELF, TA Instruments, New Castle, DE).

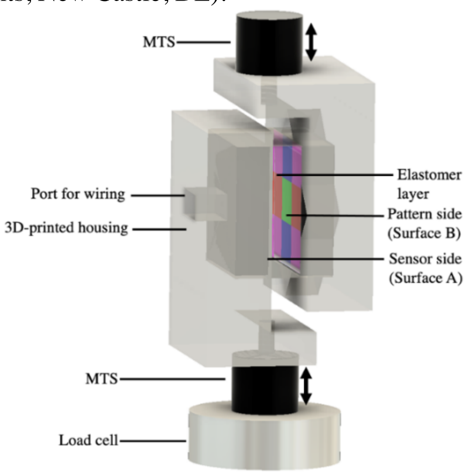

Figure 4. Rendering of experimental setup for translational testing of the sensor. The MTS actuates vertically, displacing Surface B with respect to the instrumented side of the sensor (Surface A). Displacement and force are measured via an integrated displacement sensor and load cell, respectively. Surface B can be rotated within the housing to simulate horizontal or vertical displacements.

To characterize the sensor's performance for measuring shear stress, a 3 mm-thick optically-clear PDMS elastomer layer was adhered between Surfaces A and B. The sensor was then affixed in the materials testing system using the methods described above. The sensor is effectively under no compressive load in this configuration. The materials testing system was actuated for loads ranging 0 – 20 N in 2.5 N increments, measured via a load cell (1516FQG-100, TA Instruments, New Castle, DE) placed in series with the actuator. Red, green, and blue color intensity was measured during each static load increment, as described above. To measure the repeatability of the sensor, 5 trials were completed, and inter-trial variability was calculated. Sensor-derived measurements of shear stress were then compared to data from the load cell. Hysteresis of the sensor was also characterized. All data were collected in dark conditions to avoid interference from ambient light sources.

Sensor longevity was determined through fatigue testing configured in the materials testing system (Fig. 3). The sensor was loaded from 0 – 20 N with a 1 Hz duty cycle for 10,000 cycles. The stiffness of the sensor was measured before and after the fatigue test.

Response time of the PDMS elastomer was characterized by loading the sensor (0 – 20 N) with a 1 Hz duty cycle for 10 cycles. Stress and strain data measured from the HADS and load cell onboard the MTS (f_s: 10 Hz) were plotted in the time domain. The PDMS response time was calculated as the average time offset between the stress and strain waveforms.

D. Data Analysis

Displacement data measured from the HADS (accuracy: ±0.0001 mm) and load data from the in-series load cell (accuracy: ±0.0001 N) were used as gold-standard comparator values to model and characterize the sensor's performance. The ratio R_r / R_g was used for quantifying displacement/shear stress changes in the vertical direction, whereas R_b / R_g was used for quantifying horizontal changes. For both displacement and shear stress, a model fit was derived for the sensor's response (i.e., light intensity) compared to the gold standard value.

Gaussian Process (GP) regression was used to model the sensor response for both displacement and shear stress conditions (Mathworks, Natick, MA). Compared to traditional regression models, GPs are advantageous for characterizing sensor performance because they can directly capture model uncertainty in addition to predicted values. Furthermore, the user may add *a priori* knowledge and specifications about the shape and behavior of the model by selecting different kernel functions (e.g., linear vs. exponential). Five rounds of cross-validation were performed using randomized data partitions. The validation results were averaged across the rounds to give an overall characterization of the model's predictive performance. Sensor performance was characterized using coefficient of determination (R^2), mean absolute error (MAE), and root-mean-squared error (RMSE) values across the full range of conditions tested.

III. Results and Discussion

A. Sensor Performance

Sensor-derived measurements of horizontal displacement showed a high degree of agreement with HADS values ($R^2 >$ 0.99, MAE = 0.08 mm, RMSE = 0.20 mm) (Figure 4). The sensor exhibited similar performance for vertical displacement ($R^2 > 0.99$, MAE = 0.07 mm, RMSE = 0.16 mm) (Figure 4). These data serve to demonstrate the baseline performance of the sensor's operating principle of measuring optical coupling between the RGB LED and photodiode, essentially based on the light reflected from the patterned color surface. Inter-trial variability was <0.02%, indicating that sensor strain measurements are repeatably accurate. Higher residuals (~1 mm) for displacements of 1 mm in both the horizontal and vertical directions indicate that the sensor may not be sensitive to displacements of <1 mm. For some trials, residuals were higher for displacements <5 mm, which may be due to minor experimental errors during those collections (e.g., small amounts of sensor slippage or misalignment). This parameter may be tuned through sensor design modifications such as LED light intensity or use of an amplifier.

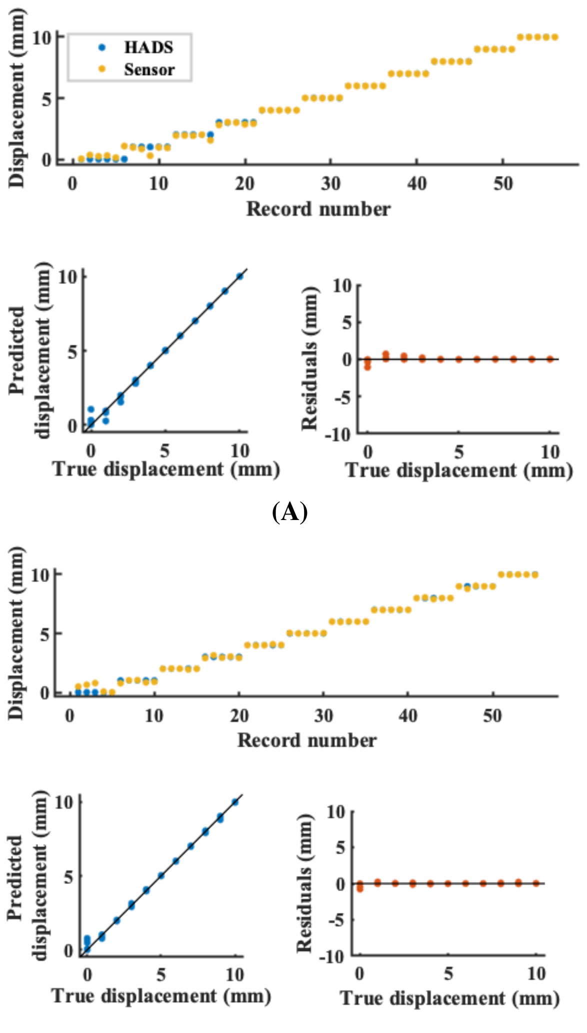

Figure 5. Performance of sensor compared to High Accuracy Displacement Sensor (HADS) for measuring **(A)** horizonal and **(B)** vertical displacements.

The sensor's performance for measuring shear stresses in the horizontal and vertical directions showed greater variability compared to the displacement measurements. Nevertheless, sensor-derived measures of horizonal shear stress matched the load cell data well with $R^2 > 0.96$, MAE = 0.97 N, and RMSE = 1.2 N (Figure 5). Performance in the vertical direction was more accurate and exhibited decreased variability compared to the horizonal direction ($R^2 > 0.98$, MAE = 0.90 N, RMSE = 0.91 N) (Figure 5). The decreased accuracy for shear measurements compared to displacement could be due to the fact that sensor fabrication was still in the prototyping stage. It is possible that the deformation of the PDMS layer was not completely homogenous, resulting in decreased accuracy for sensor-derived measurements of shear stress. It is also possible that the methods used to adhere the PDMS to Surfaces A and B were insufficient, causing some slippage during testing.

Overall, the sensor exhibited linearity of 0.98 for displacement and 0.96 for force, calculated as the slope of the relationship between sensor and gold standard values. Sensitivity was 5.1 mV/N and 3.9 mV/mm, though these values could be tuned using an amplifier circuit. The current configuration has 10 bit resolution.

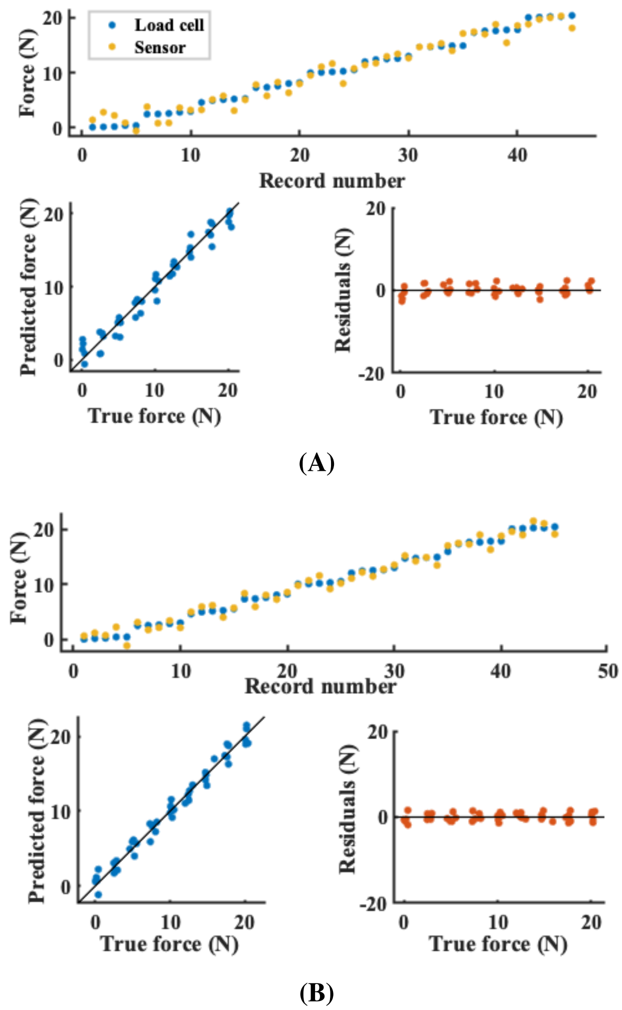

Figure 6. Performance of sensor compared to the load cell for measuring **(A)** horizonal and **(B)** vertical shear stresses.

To investigate the elastic behavior of the physical sensor package (i.e., PDMS elastomer, assuming the resin housing is rigid) the stiffness and hysteresis of the packaged sensor were evaluated. The sensor exhibited a linear relationship between load and displacement ($R^2 > 0.99$) as measured via the load cell and HADS. Hysteresis was < 0.1% across the full range of loads and displacements (Figure 6). The relationship between force (F) and displacement (x) was 13.4 N/mm and the PDMS layer has a surface area (A) of 45 mm². As such, the shear modulus (G) of the sensor's PDMS can be calculated as a function of force, displacement, and PDMS area with Eq. (1), assuming

$$G = \frac{F/x}{A} = \frac{13.4N/mm}{45mm^2} = 298\ kPa \qquad \text{Eq. (1)}$$

complete rigidity of the resin housing. The calculated modulus of 298 kPa is similar to the values reported in previous characterizations of the material properties of PDMS [14,15]. The modulus of PDMS can also be tuned based on different curing parameters [10,14,15], which makes this design scalable to meet different loading requirements. Values between

450 kPa and 930 kPa have been reported [10,14]. Scalability based on geometric variations of the elastomer layer may also be estimated using Eq. 1.

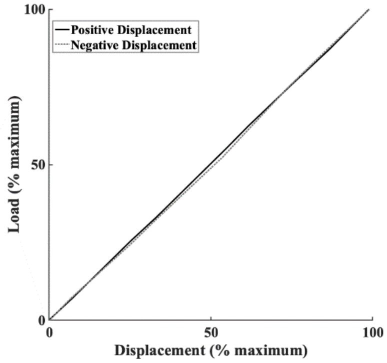

Figure 7. Hysteresis response for sensor measured via HADS and load cell.

The longevity of the sensor was evaluated through a 10,000 cycle fatigue protocol. The sensor's stiffness was 21.9 N/mm prior to fatiguing, whereas it was 20.7 N/mm afterward (-5.5% change). These data indicate that the sensor's material properties may undergo small changes with repeated loading and may necessitate periodic recalibration over the life of the sensor. Average response time of the PDMS was 0.05 s; however, error due to aliasing may have occurred due to the relatively low sampling frequency of the MTS (10 Hz).

The goal of this work is to develop a simple and low-cost shear stress sensor that meets a variety of constraints associated with use in robotics and medical applications (e.g., rehabilitation). The linearity, scalability, and resolution in shear stress measurements derived from this sensor support its use for these applications. High linearity is advantageous, as it can potentially allow for simplified sensor calibration and minimal signal conditioning requirements for data processing. The scalability is also beneficial to the adoption by other applications, as many previous shear sensor designs were limited in their uses due to low sensing range [6,9,10]. High sensor resolution is important for a variety of uses.

Data show differentiation between horizonal and vertical shear stresses and indicate that the sensor performs equally well in both directions. The quality of this technology is especially high compared to previous work in optical-based shear sensors which were only capable of sensing resultant shear stress [10–13] (Table 1). The ability to measure multi-axial shear stresses has typically been limited to strain gauges [4], [21]. However, compared to this sensor, strain gauges are often larger (e.g., 47 mm [4]), heavier (e.g., 375 g [21]), require greater power, and/or need cable tethering [20–25]. The technology shown herein exhibit both desirable sensing performance of the strain gauges and the physical/electrical characteristics of other optical sensors (Table 1).

Table 1. Comparison of sensing capacity and key design parameters.

Study	Sensing principle	Mass	Sensing capacity	Number of axes measured
Present study	Optoelectronic (Photodiode and LED)	1.01 g	Shear stress: 20 N	2: 2-axis shear stress and strain
Sanders and Daly (1992)	Metal foil strain gauge (variable resistor)	375 g	Normal pressure: 120 kPa; Shear stress: 42 kPa	2: Normal pressure and resultant shear stress
Sanders and Daly (1993)	Metal foil strain gauge (variable resistor)	*	Normal pressure: 300 kPa; Shear stress: 75 kPa	2: Normal force and resultant shear stress
Cheng et al. (2010)	Capacitance	*	Normal force: < 1 N; Shear stress: <1 N	2: Normal force and resultant shear stress
Missinne et al. (2011)	Optoelectronic (photodiode and VCSEL)	*	Shear stress: 5.5 N	1: Resultant shear stress
Laszczak et al. (2015, 2016)	Capacitance	*	Normal pressure: 400 kPa; Shear stress: 60 kPa	2: Normal pressure and resultant shear stress
Choi et al. (2019)	Capacitance	*	11 µN	2: 2-axis shear stress

*Data not reported; **VCSEL**: Vertical Cavity Surface-Emitting Laser

B. Current Limitations and Future Directions

Future work should seek to characterize the long-term performance of the sensor. It remains unclear if periodic recalibration will be necessary to account for deterioration of the elastomer layer. Similarly, the sensor's performance should be characterized under a variety of environmental conditions (e.g., temperature) congruent with intended use scenarios, as the material properties of elastomers are known to fluctuate based on varied conditions [28].

A robust characterization of the sensor's performance under a range of compressive and shear loads and loading rates will be necessary to evaluate its functionality for various use cases. The present experimental setup only allowed for evaluation of the shear sensing along the horizonal and vertical axes under effectively no compressive load. While data demonstrate the sensor's ability to differentiate between vertical and horizonal shear stresses, its capacity to correctly identify off-axis (i.e., a combination of vertical and horizonal) shearing remains unknown. Future work should test this ability. Similarly, the sensor will experience a broad range of loads and loading rates (compressive and shear) in its eventual use cases (e.g., embedded in the sole of a shoe). Its performance under these loading conditions should be evaluated.

Reducing the size of the sensor is an important next step to maximize its utility by reducing invasiveness. This could be achieved by sourcing smaller integrated circuit components and using different materials for housing, such that size can be minimized without sacrificing strength. Modifying the present sensor design to meet the requirements of different applications is also an important next step. For example, some applications may benefit from a flexible design (e.g., use within a shoe or prosthetic socket), which could be achieved through use of flexible PCBs. Currently, the use of rapid fabrication techniques (e.g., 3D printing and use of PCBs) in the construction of this sensor are advantageous for quickly designing, implementing, and testing modifications. However, future manufacturing processes may rely on traditional mass fabrication methods such as injection molding and automated circuit population to improve sensor-to-sensor repeatability and manufacturing speed. Repeatable mass fabrication of the PDMS elastomer component may also prove difficult, as PDMS material properties are sensitive to the curing conditions. This may be rectified using an alternative elastomer (e.g., thermoplastic elastomer) or individually calibrating each device.

In the future, this sensor could be implemented to provide feedback for a grasping robot to handle a fragile object by providing the necessary grip force to manipulate the object without breaking it. In clinical circumstances, pressures of <8 kPa can cause tissue ischemia [16], which necessitating high resolution for sensors tasked with preventing ischemia and skin breakdown. Shear stress has been shown to be at least equivalent to pressure as an external factor leading to tissue breakdown [17], thus supporting the use of this sensor for such applications. A potential future use case for this sensor is integration within a prosthetic socket to provide precise measurements of shear stress, which will be critical toward preventing residual limb tissue breakdown. An example of this implementation is depicted in Figure 7A. In this implementation, the sensors are integrated within a nylon mesh prosthetic socket liner at six anatomical locations known to be at risk of elevated localized shear stresses [18]–[20]. The sensors are ported via ribbon cables to a power source and control box worn outside the socket. A second potential implementation (Figure 7B) shows a wireless version of the device with an integrated Bluetooth module for sensor control and data streaming. This implementation is especially well-suited to be integrated within the insole of a shoe for measuring shearing between the foot and shoe in athletics settings or for patients with diabetic peripheral neuropathy.

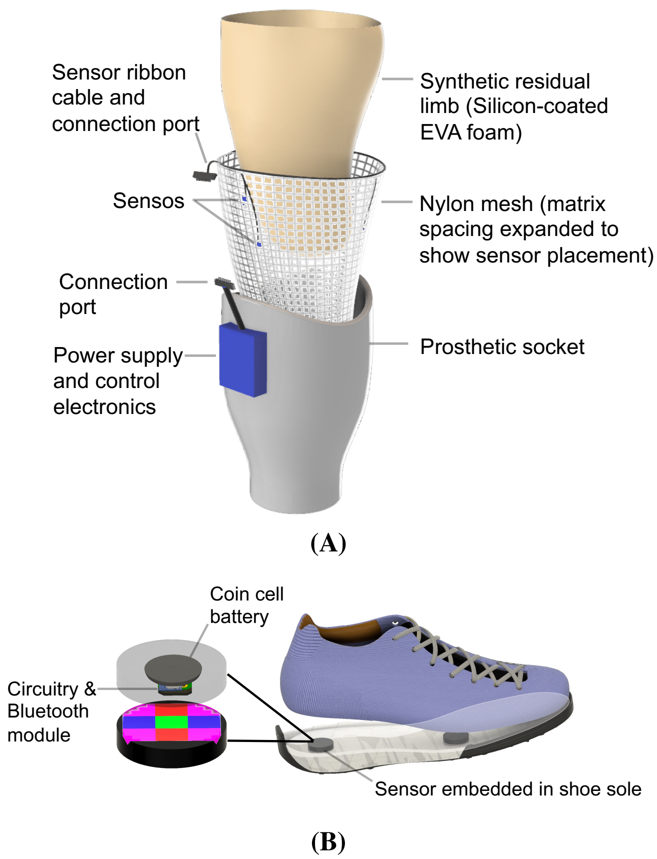

Figure 8. Potential sensor implementations: an instrumented prosthetic socket liner (**A**) and instrumented shoe insole (**B**).

IV. Conclusions

This work presented a novel method for sensing shear stress based on coupling between light from an LED reflected off a patterned color grid and a photodiode. We fabricated and characterized a sensor based on this principle. The sensor demonstrated robust and accurate measurements of multi-axial displacements and shear stresses. These properties, along with its small, low-cost, and scalable design support the use of this sensor for a variety of applications in robotics and orthopedics.

V. Acknowledgements

This work was supported by the Joe and Clara Tsai Foundation and the Wu Tsai Human Performance Alliance.

VI. References

[1] A. M. M. Yardley and K. D. Baker, “Tactile Sensors for Robots: A Review,” in *The World Yearbook of Robotics Research and Development*, Springer Netherlands, 1986, pp. 47–83.

[2] M. I. Tiwana, S. J. Redmond, and N. H. Lovell, “A review of tactile sensing technologies with applications in biomedical engineering,” *Sensors and Actuators, A: Physical*, vol. 179. Elsevier B.V., pp. 17–31, 01-Jun-2012.

[3] P. Laszczak *et al.*, “A pressure and shear sensor system for stress measurement at lower limb residuum/socket interface,” *Med. Eng. Phys.*, vol. 38, no. 7, pp. 695–700, Jul. 2016.

[4] J. E. Sanders and C. H. Daly, “Measurement of Stresses in Three Orthogonal Directions at the Residual Limb-Prosthetic Socket Interface,” *IEEE Trans. Rehabil. Eng.*, vol. 1, no. 2, pp. 79–85, 1993.

[5] P. Laszczak, L. Jiang, D. L. Bader, D. Moser, and S. Zahedi, “Development and validation of a 3D-printed interfacial stress sensor for prosthetic applications,” *Med. Eng. Phys.*, vol. 37, no. 1, pp. 132–137, Jan. 2015.

[6] M.-Y. Cheng, C.-L. Lin, Y.-T. Lai, and Y.-J. Yang, “A Polymer-Based Capacitive Sensing Array for Normal and Shear Force Measurement,” *Sensors*, vol. 10, pp. 10211–10225, 2010.

[7] R. A. Brookhuis *et al.*, “Six-axis force–torque sensor with a large range for biomechanical applications,” *J. Micromechanics Microengineering*, vol. 24, no. 3, p. 035015, Mar. 2014.

[8] J. E. Sanders, C. H. Daly, and E. M. Burgess, “Interface shear stresses during ambulation with a below-knee prosthetic limb,” *J. Rehabil. Res. Dev.*, vol. 29, no. 4, pp. 1–8, 1992.

[9] E. Choi *et al.*, “Highly sensitive tactile shear sensor using spatially digitized contact electrodes,” *Sensors (Switzerland)*, vol. 19, no. 6, Mar. 2019.

[10] J. Missinne *et al.*, “Ultra thin optical tactile shear sensor,” *Procedia Engineering*, vol. 25. Elsevier, pp. 1393–1396, 01-Jan-2011.

[11] J. Missinne *et al.*, “Flexible shear sensor based on embedded optoelectronic components,” *IEEE Photonics Technol. Lett.*, vol. 23, no. 12, pp. 771–773, 2011.

[12] J. Missinne, E. Bosman, B. Van Hoe, G. Van Steenberge, P. Van Daele, and J. Vanfleteren, “Embedded flexible optical shear sensor,” *Proc. IEEE Sensors*, pp. 987–990, 2010.

[13] J. Missinne *et al.*, “Two axis optoelectronic tactile shear stress sensor,” *Sensors Actuators, A Phys.*, vol. 186, pp. 63–68, 2012.

[14] L. C. S. Nunes, “Shear modulus estimation of the polymer polydimethylsiloxane (PDMS) using digital image correlation,” *Mater. Des.*, vol. 31, no. 1, pp. 583–588, Jan. 2010.

[15] J. C. Lötters, W. Olthuis, P. H. Veltink, and P. Bergveld, “The mechanical properties of the rubber elastic polymer polydimethylsiloxane for sensor applications,” *J. Micromechanics Microengineering*, vol. 7, no. 3, pp. 145–147, 1997.

[16] G. Allen Holloway, C. H. Daly, D. Kennedy, J. Chimoskey, C. H. Dalyjion Kennedy, and J. Cwr, “Effects of external pressure loading on human skin blood flow measured by 133Xe clearance,” 1976.

[17] M. Zhang, A. R. Turner-Smith, V. C. Roberts, and A. Tanner, “Frictional action at lower limb/prosthetic socket interface,” in *Medical Engineering and Physics*, 1996, vol. 18, no. 3, pp. 207–214.

[18] J. E. Sanders, C. H. Daly, and E. M. Burgess, “Interface shear stresses during ambulation with a below-knee prosthetic limb,” *J. Rehabil. Res.*

Dev., vol. 29, no. 4, pp. 1–8, 1992.

[19] J. E. Sanders, A. Karchin, J. R. Fergason, and E. A. Sorenson, "A noncontact sensor for measurement of distal residual-limb position during walking," *J. Rehabil. Res. Dev.*, vol. 43, no. 4, pp. 509–516, 2006.

[20] A. Courtney, M. S. Orendurff, and A. Buis, "Effect of alignment perturbations in a trans-tibial prosthesis user: A pilot study," *J. Rehabil. Med.*, vol. 48, no. 4, pp. 396–401, 2016.

[21] M. R. Safari, N. Tafti, and G. Aminian, "Socket Interface Pressure and Amputee Reported Outcomes for Comfortable and Uncomfortable Conditions of Patellar Tendon Bearing Socket: A Pilot Study," *Assist. Technol.*, vol. 27, no. 1, pp. 24–31, Jan. 2015.

[22] A. Schiff *et al.*, "Quantification of Shear Stresses Within a Transtibial Prosthetic Socket.," *Foot ankle Int.*, vol. 35, no. 8, pp. 779–782, Aug. 2014.

[23] H. Gholizadeh, N. Azuan, A. Osman, A. Eshraghi, N. Anuar, and A. Razak, "Clinical implication of interface pressure for a new prosthetic suspension system," *Biomed. Eng. Online*, vol. 13, no. 89, 2014.

[24] S. Ali, N. A. Abu Osman, A. Eshraghi, H. Gholizadeh, N. A. Bin Abd Razak, and W. A. B. Bin Wan Abas, "Interface pressure in transtibial socket during ascent and descent on stairs and its effect on patient satisfaction," *Clin. Biomech.*, vol. 28, no. 9–10, pp. 994–999, Nov. 2013.

[25] E. Boutwell, R. Stine, A. Hansen, K. Tucker, and S. Gard, "Effect of prosthetic gel liner thickness on gait biomechanics and pressure distribution within the transtibial socket," *J. Rehabil. Res. Dev.*, vol. 49, no. 2, pp. 227–240, 2012.

[26] Y. Shi, M. Hu, Y. Xing, and Y. Li, "Temperature-dependent thermal and mechanical properties of flexible functional PDMS/paraffin composites," *Mater. Des.*, vol. 185, p. 108219, Jan. 2020.

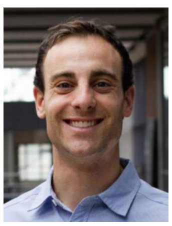

Michael A. McGeehan is a post-doctoral scholar at the University of Oregon's Phil and Penny Knight Campus for Accelerating Scientific Impact. He received the M.S. degree in 2016 and the Ph.D. degree in 2020 from the University of Oregon's Department of Human Physiology with an emphasis in biomechanics. His research areas include computational modeling, simulations, and sensor development as they relate to orthopedic rehabilitation. Dr. McGeehan's overarching research goal is to apply principles of biomechanics, physiology, and engineering toward developing rehabilitation technology that improves the lives of people with disabling conditions.

Salil Sidharthan Karipott received his B. Tech. degree in Electronics and Biomedical Engineering from Cochin University of Science and Technology in 2014. He earned his M.S. and Ph.D. degrees from the Department of Biomedical Engineering at Michigan Technological University in 2017 and 2019, respectively. He is currently a post-doctoral researcher at the Knight Campus for Accelerating Scientific Impact, University of Oregon. His work focuses on developing wireless sensing and actuating devices for orthopedic research. He has expertise in developing implantable inductive-capacitive sensors, and implementing magnetoelastic actuators for studying mechanotransduction in bone fracture healing.

Michael E. Hahn received the B.S. degree in biological sciences in 1996 from Colorado Mesa University, the M.S. degree in exercise and sports science in 2000 from Iowa State University, and the Ph.D. degree in exercise and movement science in 2003 from the University of Oregon. He served on the faculty of health and human development at Montana State University - Bozeman for five years, then as Motion Laboratory Director in the VA Puget Sound in Seattle for four years, and is currently an Associate Professor in the department of human physiology and the Director of the Bowerman Sports Science Clinic at the University of Oregon. His research interests include injury prevention and performance prediction in athletes, and design of machine learning applications in control of lower limb prostheses. He is a member of the National Academy of Inventors, serves on the editorial boards of several musculoskeletal research journals, and is the author of over 60 peer-reviewed scientific publications.

David Morgenroth is Associate Professor and Vice-Chair for Research in the Department of Rehabilitation Medicine at the University of Washington, as well as Staff Physician at VA Puget Sound Health Care System and Investigator at the VA RR&D Center for Limb Loss and Mobility (CLiMB). He received his B.S. with honors studying gait biomechanics from UC Berkeley in 1996, his M.D. from State University of New York, Brooklyn in 2003, completed residency training in Physical Medicine and Rehabilitation and a subsequent NIH-funded research fellowship at the University of Washington in 2007 and 2010, respectively. Dr. Morgenroth is a physician-scientist who focuses his clinical care and research on improving the mobility and quality of life of people with limb loss. Dr. Morgenroth serves on the Board of Trustees for the Association of Academic Physiatrists, on the Advisory Board for the Rehabilitation Medicine Scientist Training Program, and on the Editorial Board of the Archives of Physical Medicine and Rehabilitation journal.

Keat Ghee Ong received his B.S., M.S., and Ph.D. degrees in Electrical Engineering from the University of Kentucky in 1997, 1998, and 2000, respectively. He joined the department of Biomedical Engineering at Michigan Technological University, Houghton, MI in 2006. In 2019, he joined the Knight Campus for Accelerating Scientific Impact at the University of Oregon as a professor. His research areas include implantable sensors for regenerative medicine and sensor technologies for cell manufacturing. He is also working on wireless sensor networks, magnetoelastic materials, and measurement technique and instrument automation. Ong is a senior member of National Academy of Inventors. He is on the editorial boards of multiple sensor related journals, and is the author of over 100 publications in archival journals.